place limits, finding the companion to be at least 2,000 K hotter than the disk.

We detected the secondary at multiple epochs and the components show no apparent relative motion greater than 15 mas yr^{-1}. As it seems reasonable to assume that the two objects do form a bound pair, assuming a total system mass of $\sim 10 M_{\odot}$ results in an orbital period of 49 yr, given a physical separation of 28.8 AU. The apparent motion exhibited by such a system is comparable to our limit, and so extra observations at future epochs should reveal the orbit of this system. We hope such future observations, and the extension of imaging to shorter wavelengths, will help to identify which component provides the ionizing flux powering this young active region. □

Received 3 October; accepted 28 December 2000.

1. Terebey, S., Shu, F. H. & Cassen, P. The collapse of the cores of slowly rotating isothermal clouds. *Astrophys. J.* **286,** 529–551 (1984).
2. Yorke, H. W., Bodenheimer, P. & Laughlin, G. The formation of protostellar disks. 2: Disks around intermediate-mass stars. *Astrophys. J.* **443,** 199–208 (1995).
3. Cassen, P. M., Smith, B. F., Miller, R. H. & Reynolds, R. T. Numerical experiments on the stability of preplanetary disks. *Icarus* **48,** 377–392 (1981).
4. Shu, F. H., Tremaine, S., Adams, F. C. & Ruden, S. P. Sling amplification and eccentric gravitational instabilities in gaseous disks. *Astrophys. J.* **358,** 495–514 (1990).
5. Hollenbach, D., Johnstone, D., Lizano, S. & Shu, F. Photoevaporation of disks around massive stars and application to ultracompact H II regions. *Astrophys. J.* **428,** 654–669 (1994).
6. Hillenbrand, L. A., Strom, S. E., Vrba, F. J. & Keene, J. Herbig Ae/Be stars—Intermediate-mass stars surrounded by massive circumstellar accretion disks. *Astrophys. J.* **397,** 613–643 (1992).
7. Kessel, O., Yorke, H. W. & Richling, S. Photoevaporation of protostellar disks. III. The appearance of photoevaporating disks around young intermediate mass stars. *Astron. Astrophys.* **337,** 832–846 (1998).
8. Hartmann, L., Kenyon, S. J. & Calvet, N. The excess infrared emission of Herbig Ae/Be stars—Disks or envelopes? *Astrophys. J.* **407,** 219–231 (1993).
9. Böhm, T. & Catala, C. Forbidden lines in Herbig Ae/Be stars: the [O I](1F) 6300.31Å and 6363.79Å lines. I. Observations and qualitative analysis. *Astron. Astrophys.* **290,** 167–175 (1994).
10. Miroshnichenko, A., Ivezic, Z. & Elitzur, M. On protostellar disks in Herbig Ae/Be stars. *Astrophys. J.* **475,** L41–L44 (1997).
11. Pezzuto, S., Strafella, F. & Lorenzetti, D. On the circumstellar matter distribution around Herbig Ae/Be stars. *Astrophys. J.* **485,** 290–307 (1997).
12. Miroshnichenko, A., Ivezic, Z., Vinkovic, D. & Elitzur, M. Dust emission from Herbig Ae/Be stars: evidence for disks and envelopes. *Astrophys. J.* **529,** L115–L118 (1999).
13. Barsony, M., Scoville, N. Z., Schombert, J. M. & Claussen, M. J. The circumstellar environment of the emission-line star LkH-alpha 101. *Astrophys. J.* **362,** 674–690 (1990).
14. Hou, J., Jiang, D. & Fu, C. Physical properties of stellar winds from young stellar objects. *Astron. Astrophys.* **327,** 725–735 (1997).
15. Tuthill, P. G., Monnier, J. D., Danchi, W. C., Wishnow, E. H. & Haniff, C. A. Michelson interferometry with the Keck I telescope. *Publ. Astron. Soc. Pacif.* **112,** 555–565 (2000).
16. Barsony, M., Schombert, J. M. & Kis-Halas, K. The LkH-alpha 101 infrared cluster. *Astrophys. J.* **379,** 221–231 (1991).
17. Herbig, G. H. The spectrum of LkHα 101 in the near-infrared. *Astrophys. J.* **169,** 537–541 (1971).
18. Stine, P. C. & O'Neal, D. Radio emission from young stellar objects near LkHα 101. *Astron. J.* **116,** 890–894 (1998).
19. Harris, S. 5 GHz radio observations of LkHα 101, M1-82#1 and other infrared sources. *Mon. Not. R. Astron. Soc.* **174,** 601–607 (1976).
20. Cohen, M., Bieging, J. H. & Schwartz, P. R. VLA observations of mass loss from T Tauri stars. *Astrophys. J.* **253,** 707–715 (1982).
21. Panagia, N. Some physical parameters of early-type stars. *Astron. J.* **78,** 929–934 (1973).
22. Millan-Gabet, R. *et al.* Sub-astronomical unit structure of the near-infrared emission from AB Aurigae. *Astrophys. J.* **513,** L131–L134 (1999).
23. Millan-Gabet, R., Schloerb, F. P. & Traub, W. A. Spatially resolved circumstellar structure of Herbig Ae/Be stars in the near-infrared. *Astrophys. J.* **546,** 358–381 (2001).
24. Akeson, R. L. *et al.* Infrared interferometric observations of young stellar objects. *Astrophys. J.* **543,** 313–317 (2000).
25. Gull, S. F. & Skilling, J. Maximum entropy method in image processing. *IEE Proc. F* **131,** 646–650 (1984).
26. Sivia, D. S. *Phase Extension Methods.* Thesis, Cambridge Univ. (1987).
27. Tuthill, P. G., Monnier, J. D. & Danchi, W. C. A dusty pinwheel nebula around the massive star WR 104. *Nature* **398,** 487 (1999).
28. Tuthill, P. G., Monnier, J. D., Danchi, W. C. & Lopez, B. Smoke signals from IRC + 10216: 1. Milliarcsecond proper motions of the dust. *Astrophys. J.* **543,** 284 (2000).
29. Lynden-Bell, D. & Pringle, J. E. The evolution of viscous discs and the origin of the nebular variables. *Mon. Not. R. Astron. Soc.* **168,** 603–637 (1974).

Acknowledgements

We would like to thank D. Sivia for the maximum-entropy mapping program VLBMEM. Data were obtained at the W.M. Keck Observatory, made possible by the generous support of the W.M. Keck Foundation, operated as a scientific partnership among the California Institute of Technology, the University of California and NASA. This work was supported through grants from the National Science Foundation.

Correspondence and requests for materials should be addressed to P.T. (e-mail: gekko@physics.usyd.edu.au).

Experimental entanglement distillation and 'hidden' non-locality

Paul G. Kwiat*†, Salvador Barraza-Lopez*†, André Stefanov‡ & Nicolas Gisin‡

* *Physics Division, P-23, Los Alamos National Laboratory, Los Alamos, New Mexico 87545, USA*

‡ *Group of Applied Physics, University of Geneva, 1211 Geneva 4, Switzerland*

Entangled states are central to quantum information processing, including quantum teleportation[1], efficient quantum computation[2] and quantum cryptography[3]. In general, these applications work best with pure, maximally entangled quantum states. However, owing to dissipation and decoherence, practically available states are likely to be non-maximally entangled, partially mixed (that is, not pure), or both. To counter this problem, various schemes of entanglement distillation, state purification and concentration have been proposed[4–11]. Here we demonstrate experimentally the distillation of maximally entangled states from non-maximally entangled inputs. Using partial polarizers, we perform a filtering process to maximize the entanglement of pure polarization-entangled photon pairs generated by spontaneous parametric down-conversion[12,13]. We have also applied our methods to initial states that are partially mixed. After filtering, the distilled states demonstrate certain non-local correlations, as evidenced by their violation of a form of Bell's inequality[14,15]. Because the initial states do not have this property, they can be said to possess 'hidden' non-locality[6,16].

The basic idea of distillation is to extract from an ensemble of pairs of non-maximally entangled qubits a smaller number of pairs with a higher degree of entanglement. In the literature and the scientific community this procedure has also been described as 'purification' and 'concentration'. We adopt the term 'distillation', following refs 7 and 9 and others, as most descriptive of the nature of the process. Following ref. 11, we reserve 'purification' for processes which increase purity, but not entanglement; and 'concentration' for processes which increase both.

Because the qubits may be separated in space, only local operations and classical communication (LOCC) are allowed. The simplest procedure—Bernstein's 'procrustean method'[4]—is as follows. A two-qubit state of the form

$$|\phi_\epsilon\rangle = (\epsilon|00\rangle + |11\rangle)/\sqrt{1+\epsilon^2}, \qquad (1)$$

which is non-maximally entangled for $\epsilon \neq 1$, can be transformed into the maximally entangled state $|\phi^+\rangle = |00\rangle + |11\rangle$ (unnormalized), simply by subjecting one of the qubits to a generalized measurement[17–19] that takes $|0\rangle \rightarrow |0\rangle$ and $|1\rangle \rightarrow \epsilon|1\rangle$. This nonunitary filtering process equalizes the contribution of the two terms in equation (1), thereby yielding perfect entanglement. Such a procedure is the necessary first step in a distillation protocol known to apply to all entangled two-qubit states[7].

Our set-up to investigate procrustean distillation is shown in Fig. 1. As described elsewhere[13], using two adjacent nonlinear crystals (β-barium borate, BBO), we can readily produce photon pairs in any state of the form $|\phi_\epsilon\rangle = (\epsilon|\,\mathrm{HH}\,\rangle + |\,\mathrm{VV}\rangle)/\sqrt{1+\epsilon^2}$, where H and V represent horizontal and vertical polarization (coding for qubits $|0\rangle$ and $|1\rangle$), respectively. The basic principle of the source is that an incident ultraviolet pump photon may be split into two infrared photons either in the first crystal (from the pump's vertical polarization component), in which case the daughter

† Present addresses: University of Illinois, Urbana-Champaign, Department of Physics, 1110 West Green Street, Urbana, Illinois 61801-3080, USA (P.G.K.); Escuela Superior de Física y Matemáticas, IPN, Mexico D.F., 07738, Mexico (S.B.-L.).

photons are both horizontally polarized; or in the second crystal (from the pump's horizontal polarization component), in which case they are vertically polarized. Owing to the coherent nature of the process, and the fact that the output spatial modes of the photons are nearly identical, the photons produced in this way can exhibit almost perfect polarization-entanglement[12]. By simply varying the pump polarization, we can arbitrarily set ϵ.

The photons are detected in coincidence using silicon avalanche photodiodes, thereby projecting out the large vacuum state from the possibility of the pump photon not downconverting, and selecting the two-photon contribution to the total quantum mechanical state. (In our experiment the residual contribution from higher-order processes, that is, with simultaneous multiple pairs, is less than 0.1%.) We thus restrict our discussion to this two-photon subspace. The polarization of each photon may be analysed in an arbitrary basis, by means of a quarter wave plate (QWP), half wave plate (HWP), and polarizing beam splitter (PBS) in each arm. By making 16 measurements of the polarization correlations in various bases (for example, HH, HV, 45° V, and so on), which are essentially the two-photon analogues of the classical Stoke's parameters[20], we may derive the density matrix describing the polarization state of the pairs produced[13]. Figure 2a (left) shows typical data, corresponding to the state $0.41|\mathrm{HH}\rangle + 0.91|\mathrm{VV}\rangle$, for which $\epsilon = 0.45$.

The procrustean filtering can be realized experimentally by inserting into one path a series of coated glass slabs, tilted about the vertical axis by 58° (approximately Brewster's angle for these slabs). Owing to the well known polarization-dependent reflectivity[20], the transmitted photons are preferentially horizontally polarized. Specifically, with four slabs, the transmission probability for horizontal polarization was $T_H = 0.89$, while for vertical polarization it was only $T_V = 0.18$. The state ρ_{out} after filtering is shown in Fig. 2a (right). Its fidelity with the maximally entangled state $|\phi^+\rangle = (|\mathrm{HH}\rangle + |\mathrm{VV}\rangle)/\sqrt{2}$ (defined as $Tr[\langle\phi^+|\rho_{out}|\phi^+\rangle]$) is 0.99 ± 0.04, indicating a successful distillation. We performed similar distillation for several values of ϵ, changing our partial polarizers accordingly; in every case the fidelity of the resulting density matrix with the desired maximally-entangled state $|\phi^+\rangle$ was close to 1.

The efficiency of the procrustean method—the probability that a given input pair survives the filtering process—is directly linked to the value of ϵ, that is, to the required amount of distillation. In an ideal system we would have $T_H = 1$, $T_V = \epsilon^2$, so that the yield of output maximally entangled pairs is $2\epsilon^2/(1+\epsilon^2)$. In our experiment, the values of T_H were slightly less than one, because of some absorption in the InSnO coating on our glass slabs. Our measured efficiencies are plotted in Fig. 2b, along with the ideal theoretical prediction, and the expectation based on our actual measured values of T_H and T_V. Remarkably, this simplest method of distillation always has a higher yield/input pair than more complicated (and presently physically unrealizable) schemes relying on jointly processing n pairs, as long as $n \leqslant 5$ (ref. 4): for the particular non-maximally entangled states we studied ($\epsilon = 0.45$, 0.68, 0.77 and 0.90) our observed yields are superior unless $n \geqslant 5$, 10, 9 and 28, respectively.

Before coming to the more general case, let us emphasize the difference between the distillation filtering process and the post-selection done by the detectors. The former necessarily depends on the photon polarization to select out a particular subensemble of pairs of photons from the initial total ensemble of pairs; this filtering affects the state, that is, it changes the relative weightings within the two-photon density matrix. In contrast, the detectors merely reveal the two-photon component of the state, by selecting pairs out of an initial superposition of photons and no-photons (that is, the vacuum); this post-selection is made independently of all analysis settings, as the detector efficiencies do not depend on polarization. If this were not so, we could observe apparently non-local effects from completely classical ensembles[6,16].

Next consider the situation of an initial state that is partially mixed, in addition to being non-maximally entangled:

$$\rho_{\epsilon,\lambda} = \lambda|\phi_\epsilon\rangle\langle\phi_\epsilon| + \frac{(1-\lambda)}{2}(|\mathrm{HV}\rangle\langle\mathrm{HV}| + |\mathrm{VH}\rangle\langle\mathrm{VH}|) \qquad (2)$$

The first term corresponds to a pure, non-maximally entangled component, the second to a mixed component. One feature of

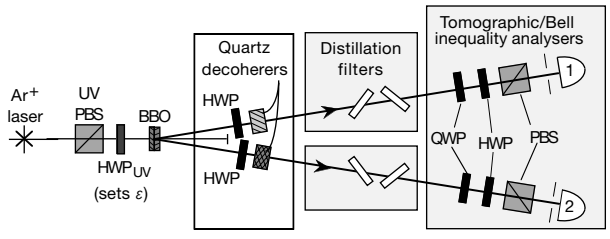

Figure 1 Experimental set-up used to investigate entanglement distillation and hidden non-locality. Spontaneous down-conversion in two adjacent β-barium borate (BBO) crystals results in polarization-entangled photons. The initial degree of entanglement ϵ is determined by the linear polarization angle θ of the pump beam (at 351 nm, from an argon ion laser): $\epsilon = \tan\theta$. In the experiment requiring partial mixture as well, each photon is passed through an adjustable half wave plate (HWP) and a 1-cm-thick quartz element, to introduce decoherence in a particular basis. The final quarter wave plate (QWP) and half wave plate in each arm, along with polarizing beamsplitters (PBS), enable analysis of the polarization correlations in any basis, allowing tomographic reconstruction of the density matrix, and measurement of Bell's inequalities. The distillation filters comprise glass substrates, tilted near Brewster's angle, and symmetrically arranged in pairs to compensate for transverse displacements. The result is an adjustable ratio of the transmissions for vertical and horizontal polarization. In the experimental to concentrate entanglement from a non-maximally entangled state, filtering was performed in one arm only. In the experiment on hidden non-locality, identical filters were placed in each arm, as shown.

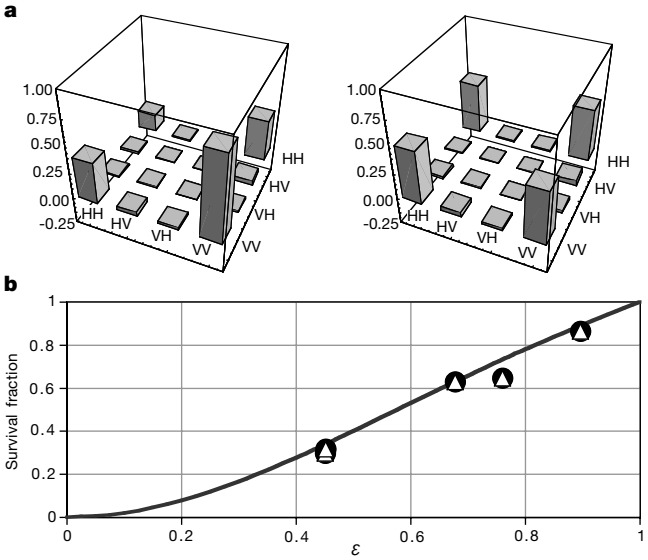

Figure 2 Experimental results showing entanglement distillation of non-maximally entangled states. **a**, Left is the measured two-photon polarization density matrix for the initial, unfiltered state: $0.41|\mathrm{HH}\rangle + 0.91|\mathrm{VV}\rangle$; right is the resulting maximally-entangled state after an appropriate generalized filtering measurement has been performed. (Only the real parts are shown; the imaginary components, which theoretically are strictly zero, were typically less than 1%.) **b**, The fractional 'survival' probability is plotted as a function of the initial degree of entanglement ϵ. The solid curve is the theoretical prediction under the optimal condition where T_H of the filter is 1. Our data points (solid circles) are well predicted by a theory (open triangles) using our actual measured values of T_H (typically ~0.92) and T_V.

Table 1 Summary of distillation data for testing Bell's inequalities

Trial	ϵ_{non}	λ_{non}	S_{non}^{calc}	S_{non}^{exp}	$\epsilon_{filtered}$	$\lambda_{filtered}$	$S_{filtered}^{calc}$	$S_{filtered}^{exp}$
1	0.46	0.78	1.63 ± 0.04	1.60 ± 0.02	1.02	0.73	2.02 ± 0.04	2.02 ± 0.03
2	0.47	0.83	1.81 ± 0.04	1.82 ± 0.02	1.01	0.79	2.20 ± 0.04	2.22 ± 0.03
3	0.47	0.87	1.96 ± 0.04	1.94 ± 0.02	0.99	0.83	2.31 ± 0.04	2.34 ± 0.02

The table shows the measured ϵ and λ parameters of the non-filtered and filtered states, and the calculated and experimentally measured S values. The errors in the latter are calculated from Poisson statistics. The calculated predictions for S were obtained by averaging S over an ensemble of density matrices slightly deviated from the ideal state corresponding to ϵ and λ.

entangled quantum systems is that some of the correlations they predict cannot be explained by an local realistic model. This statement is made more quantitative by Bell's inequalities (BI)[14]. Here we shall always restrict our discussion to the Clauser–Horne–Shimony–Holt (CHSH) version[15] (and its equivalents), though in general there may exist more revealing tests of non-locality, for example, ones which rely on sequences of measurements on each particle[16]. The CHSH inequality places constraints on the value of S, a combination of four polarization correlation probabilities—two possible analysis settings for each photon. If $|S| \leqslant 2$, no quantum mechanical entanglement is necessary to explain the correlations, that is, some local model can reproduce them. For a maximally-entangled state the maximum value of $S = 2\sqrt{2}$. The optimal analysis settings for a particular state ρ may be determined, for example by using the analytical method of ref. 21. Depending on the values of ϵ and λ, $\rho_{\epsilon,\lambda}$ may be unable to violate any CHSH inequality[6], for instance, if the state is too mixed ($\lambda \leqslant 1/\sqrt{2}$). Figure 3 indicates the ranges over which no CHSH BI can be violated.

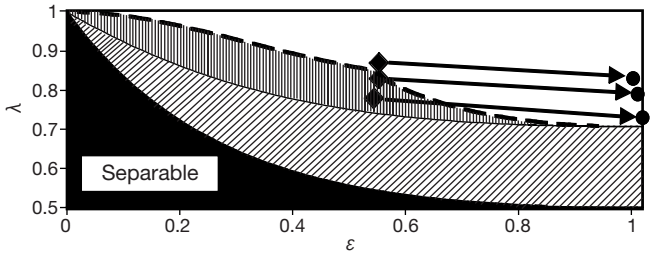

Figure 3 Contour plots in the ϵ–λ plane, showing the curves for $S = 2$, for states of the form (2). The dashed curve corresponds to the unfiltered state; below this line one cannot violate a Bell's inequality of the CHSH-type. The solid curve shows the $S = 2$ threshold for states after an optimal distillation of the filtering sort described here—no CHSH violation is ever possible in the lower, diagonally-hatched region below this curve. The vertically-hatched overlap region indicates states possessing 'hidden' non-locality—a local filtering operation enables one to violate a suitable Bell's inequality. Finally, the solid region at the bottom shows states which are completely separable, that is, no entanglement can ever by recovered by only local operations and classical communication. The diamonds indicate the initial values for our three experimental trials (see Table 1); the circles are the post-distillation values.

The process of distillation can alter this, however. The filtering method is similar to that described above, except that now we make a generalized measurement in each arm. Specifically, if each partial polarizer has $T_H = 1$ and $T_V = \epsilon$, the state (2) becomes (up to a normalization factor):

$$\frac{2\epsilon^2\lambda}{1+\epsilon^2}|\phi^+\rangle\langle\phi^+| + \frac{\epsilon(1-\lambda)}{2}(|HV\rangle\langle HV| + |VH\rangle\langle VH|) \qquad (3)$$

We note that the relative contribution of the entangled term has been reduced by a factor of $2\epsilon/(1+\epsilon^2)$—the filtered state (3) is more mixed than the original $\rho_{\epsilon,\lambda}$. Nevertheless, because the remaining pure component is now maximally entangled, the state may violate a suitable BI (Fig. 3).

The method to experimentally produce generalized states as in state (2) is discussed elsewhere[22,23]. By sending each photon through a thick birefringent element (~1 cm quartz), we introduce a frequency-dependent phase offset between two polarization components. As this offset is greater than the coherence length of the photons (~100 μm, in our case determined by the 5-nm (full width at half maximum) interference filter in front of the detector), the resulting polarization quantum state of the pair can be mixed. The birefringent element acts to entangle the polarization and frequency degrees of freedom; when we trace over the frequency (since the detectors are insensitive to wavelength over the collection bandwidth), the reduced density matrix for polarization becomes mixed[23]. By appropriately adjusting the pump polarization (with HWP_{UV}) and the decoherence basis (with half wave plates before the quartz), we can prepare states of the form $\rho_{\epsilon,\lambda}$.

We investigated distillation on several different starting states (see Table 1). From a tomographically measured density matrix of each initial, unfiltered state, we analytically and numerically determine QWP and HWP analysis settings predicting the maximum S value. We then measure S directly using these (16) settings, and the normalization procedure introduced in ref. 24. The first trial corresponds to a state which clearly does not violate any CHSH inequality, but is just at the limit when filtered. In the second trial there is a definite transition between no initial violation and violation after filtering (Figs 4a and b show the density matrices before and after filtering, respectively). The final trial starts with a state which is near the threshold of violation, and ends with a strong violation (17σ). To our knowledge, this is the first time Bell's inequalities have been tested using mixed states.

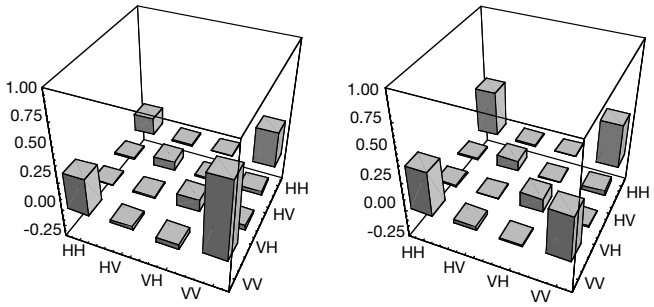

Figure 4 Density matrices for states displaying 'hidden' non-locality. The initial state (left) is $0.83\rho_{0.43HH+0.90W} + 0.09(\rho_{HV} + \rho_{VH})$. After symmetric filtering, the state is transformed (right) into one which is $0.79\rho_{0.71HH+0.71W} + 0.11(\rho_{HV} + \rho_{VH})$. We note that the purity, defined as $Tr[\rho^2]$, is actually reduced from 0.69 to 0.64 by the distillation process, that is, the final state is more mixed than the initial.

Whereas our distillation procedure employs only local operations (filtering) and classical communication (coincidence counting), our non-locality demonstrations clearly rely on 'conditional probabilities'[16,25]—we include only events in which both photons are transmitted by their respective partial polarizers. Nevertheless, we emphasize that these filters are before the analysers, and are thus independent of the polarization measurements. The filtering process is used to select a particular subensemble of the original states. The entanglement for members of this subensemble (corresponding to coincident detections) is higher than the average for the entire ensemble (which includes photons reflected at the partial polarizers—these possess no entanglement whatsoever), and therefore they are able to demonstrate non-local effects, such as violations of Bell's inequalities. This is completely consistent with the fact that LOCC cannot be used to increase the average entanglement of an ensemble[4]. For instance, for our second trial, the initial degree of entanglement (of formation)[26] before filtering is $E = 0.32$; after filtering the transmitted photons have $E = 0.44$, but the reflected photons have $E = 0$. □

Received 11 September; accepted 15 December 2000.

1. Bennet, C. H. *et al.* Teleporting an unknown quantum state via dual classical and Einstein–Podolsky–Rosen channels. *Phys. Rev. Lett.* **70,** 1895–1899 (1992).
2. Bennett, C. & DiVincenzo, D. P. Quantum information and computation. *Nature* **404,** 247–255 (2000).
3. Ekert, A. K. Quantum cryptography based on Bell theorem. *Phys. Rev. Lett.* **67,** 661–663 (1991).
4. Bennett, C. H., Bernstein, H. J., Popescu, S. & Schumacher, B. Concentrating partial entanglement by local operations. *Phys. Rev. A* **53,** 2046–2052 (1996).
5. Bennett, C. H. *et al.* Purification of noisy entanglement and faithful teleportation via noisy channels. *Phys. Rev. Lett.* **76,** 722–725 (1996).
6. Gisin, N. Hidden quantum nonlocality revealed by local filters. *Phys. Lett. A* **210,** 151–156 (1996).
7. Horodecki, M., Horodecki, P. & Horodecki, R. Inseparable two spin-1/2 density matrices can be distilled to a singlet form. *Phys. Rev. Lett.* **78,** 574–577 (1997).
8. Linden, N., Massar, S. & Popescu, S. Purifying noisy entanglement requires collective measurements. *Phys. Rev. Lett.* **81,** 3279–3282 (1998).
9. Opatrny, T. & Kurizki, G. Optimization approach to entanglement distillation. *Phys. Rev. A* **60,** 167–172 (1999).
10. Bose, S., Vedral, V. & Knight, P. L. Purification via entanglement swapping and conserved entanglement. *Phys. Rev. A* **60,** 194–197 (1999).
11. Thew, R. T. & Munro, W. J. Entanglement manipulation and concentration. *Phys. Rev. A* (in the press); also preprint quant-ph/0012049 at ⟨xxx.lanl.gov⟩ (2000).
12. Kwiat, P. G., Waks, E., White, A. G., Appelbaum, L. & Eberhard, P. H. Ultrabright source of polarization-entangled photons. *Phys. Rev. A* **60,** R773–R776 (1999).
13. White, A. G., James, D. F. V., Eberhard, P. H. & Kwiat, P. G. Nonmaximally entangled states: Production, characterization, and utilization. *Phys. Rev. Lett.* **83,** 3103–3107 (1999).
14. Bell, J. S. On the Einstein-Podolsky-Rosen paradox. *Physics* **1,** 195 (1965).
15. Clauser, J., Horne, M., Shimony, S. & Holt, R. Proposed experiment to test local hidden-variable theories. *Phys. Rev. Lett.* **23,** 880–884 (1969).
16. Popescu, S. Bell's inequalities and density matrices: Revealing 'hidden' nonlocality. *Phys. Rev. Lett.* **74,** 2619–2622 (1995).
17. Helstrom, C. W. Quantum Detection and Estimation Theory (Academic, New York, 1976).
18. Huttner, B. *et al.* Unambiguous quantum measurement of non-orthogonal states. *Phys. Rev. A* **54,** 3783–3789 (1996).
19. Clark, R. B. M., Chefles, A., Barnett, S. M. & Riis, E. Experimental demonstration of optimal unambiguous state discrimination. *Phys. Rev. A* (in the press); preprint quant-ph/0007063 at ⟨xxx.lanl.gov⟩ (2000).
20. Born, M. & Wolf, E. *Principles of Optics* 30–32 (Cambridge Univ. Press, Cambridge, 1999).
21. Horodecki, R., Horodecki, P. & Horodecki, M. Violating Bell inequality by mixed spin-1/2 states: Necessary and sufficient condition. *Phys. Lett. A* **200,** 340–344 (1995).
22. Kwiat, P. G., Berglund, A. J., Altepeter, J. B. & White, A. G. Experimental verification of decoherence-free subspaces. *Science* **290,** 498–501 (2000).
23. Berglund, A. J. *Quantum Coherence and Control in One- and Two-Photon Optical Systems.* Thesis, Dartmouth College B.A. (2000); also preprint quant-ph/0010001 at ⟨xxx.lanl.gov⟩ (2000).
24. Aspect, A., Grangier, P. & Roger, G. Experimental realization of Einstein–Podolsky–Rosen–Bohm *gedankenexperiment*: A new violation of Bell's inequalities. *Phys. Rev. Lett.* **49,** 91–94 (1982).
25. Zukowski, M., Horodecki, R., Horodecki, M. & Horodecki, P. Generalized quantum measurements and local realism. *Phys. Rev. A* **58,** 1694–1698 (1998).
26. Wootters, W. K. Entanglement of formation of an arbitrary state of two qubits. *Phys. Rev. Lett.* **80,** 2245–2248 (1998).

Acknowledgements

We thank H. Bernstein, D. DiVincenzo, B.-G. Englert, L. Hardy, D. James and M. Zukowski for helpful discussions. This work was supported in part by the National Security Agency (NSA) and Advanced Research and Development Activity (ARDA), and by the European IST FET QuComm project.

Correspondence and requests for materials should be addressed to P.G.K. (e-mail: Kwiat@uiuc.edu).

Fluid particle accelerations in fully developed turbulence

A. La Porta, Greg A. Voth, Alice M. Crawford, Jim Alexander & Eberhard Bodenschatz

Laboratory of Atomic and Solid State Physics, Laboratory of Nuclear Studies, Cornell University, Ithaca, New York 14853-2501, USA

The motion of fluid particles as they are pushed along erratic trajectories by fluctuating pressure gradients is fundamental to transport and mixing in turbulence. It is essential in cloud formation and atmospheric transport[1,2], processes in stirred chemical reactors and combustion systems[3], and in the industrial production of nanoparticles[4]. The concept of particle trajectories has been used successfully to describe mixing and transport in turbulence[3,5], but issues of fundamental importance remain unresolved. One such issue is the Heisenberg–Yaglom prediction of fluid particle accelerations[6,7], based on the 1941 scaling theory of Kolmogorov[8,9]. Here we report acceleration measurements using a detector adapted from high-energy physics to track particles in a laboratory water flow at Reynolds numbers up to 63,000. We find

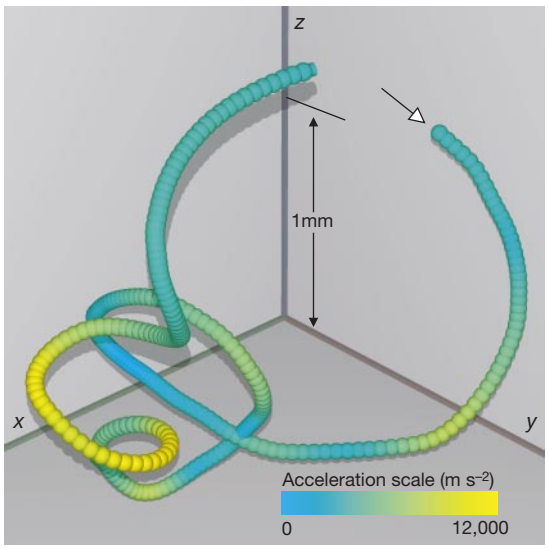

Figure 1 Measured particle trajectory. The three-dimensional time-resolved trajectory of a 46-μm-diameter particle in a turbulent water flow at Reynolds number 63,000 ($R_\lambda = 970$). A sphere marks the measured position of the particle in each of 300 frames taken every 0.014 ms ($\approx \tau_\eta/20$). The shading indicates the acceleration magnitude, with the maximum value of 12,000 m s^{-2} corresponding to approximately 30 standard deviations. The turbulence is generated between coaxial counter-rotating disks[24,25] in a closed-flow chamber of volume 0.1 m^3 with rotation rates ranging from 0.15 Hz to 7.0 Hz, giving r.m.s. velocity fluctuation $\tilde{u}$ in the range $0.018\,\mathrm{m\,s^{-1}} < \tilde{u} < 0.87\,\mathrm{m\,s^{-1}}$. Measurements are made in an 8-mm^3 volume at the centre of the apparatus where the mean velocity is zero and the flow is nearly homogeneous but not isotropic. As a result of a mean stretching of the flow along the propeller axis the r.m.s. fluctuations are one-third larger for the transverse velocity components than for the axial component. The energy dissipation was determined from measurements of the transverse second-order structure function D_{NN} and the Kolmogorov relation $D_{NN} = \frac{4}{5} C_1 (\epsilon r)^{2/3}$ with $C_1 = 2.13$ (ref. 26), ϵ the turbulent energy dissipation, and r the particle separation. The dissipation was found to be related to the r.m.s. velocity fluctuation by $\epsilon = \tilde{u}^3/L$ with an energy injection scale $L = (71 \pm 7)$ mm. Using the definition of the Taylor microscale Reynolds number $R_\lambda = (15 \tilde{u} L/\nu)^{1/2}$, the range of Reynolds numbers accessible is $140 \leqslant R_\lambda \leqslant 970$ (in terms of the classical Reynolds number $1{,}300 \leqslant \mathrm{Re} \leqslant 63{,}000$). At the highest Reynolds number the system is characterized by Kolmogorov distance and timescales of $\eta = 18$ μm and $\tau_\eta = 0.3$ ms, respectively.